Mechanism of transport modulation by an extracellular loop in an archaeal Excitatory Amino Acid Transporter (EAAT) homolog

Christopher Mulligan and Joseph A. Mindell

Membrane Transport Biophysics Section, Porter Neuroscience Research Center, National Institute of Neurological Disorders and Stroke, National Institutes of Health, Bethesda, MD 20892

Running title: Loop cleavage inhibits conformational change in Glt_{Ph}

To whom correspondence should be addressed: Joseph A. Mindell, Membrane Transport Biophysics Section, Porter Neuroscience Research Center, National Institute of Neurological Disorders and Stroke, National Institutes of Health, Bethesda, MD 20892, USA. Tel.: (301) 402-3473; e-mail: mindellj@ninds.nih.gov.

Key words: Protein crosslinking; membrane transport, reconstitution of membrane transporters; amino acids transport; glutamate; transporters; chemical modification

Background The extracellular loop, 3L4, plays an important, unknown role in the transport cycle of the glutamate transporter homolog, Glt_{Ph}.
Results Cleaving 3L4 differentially affects transport cycle steps.
Conclusion 3L4 discriminates between substrate-loaded and empty states of the transporter.
Significance Empty and loaded forms of the transport domain have structurally distinguishable forms, reflecting essential features of the transport mechanism.

ABSTRACT

Secondary transporters in the excitatory amino acid transporters (EAATs) family terminate glutamatergic synaptic transmission by catalyzing Na^+-dependent removal of glutamate from the synaptic cleft. Recent structural studies of the aspartate-specific, archaeal homolog, Glt_{Ph}, suggest that transport is achieved by a rigid body, piston-like movement of the transport domain, which houses the substrate binding site, between the extracellular and cytoplasmic sides of the membrane. This transport domain is connected to an immobile scaffold by 3 loops, one of which, the 3-4 loop (3L4), undergoes substrate sensitive conformational change. Proteolytic cleavage of the 3L4 was found to abolish transport activity indicating an essential function for this loop in the transport mechanism. Here, we demonstrate that despite the presence of fully cleaved 3L4, Glt_{Ph} is still able to sample conformations relevant for transport. Optimized reconstitution conditions reveal that fully cleaved Glt_{Ph} retains some transport activity. Analysis of the kinetics and temperature dependence of transport accompanied by direct measurements of substrate binding reveal that this decreased transport activity is not due to alteration of the substrate binding characteristics, but is caused by significantly reduced turnover rate. By measuring solute counterflow activity and crosslink formation rates, we demonstrate that cleaving 3L4 severely and specifically compromises one or more steps contributing to the movement of the substrate-loaded transport domain between the outward- and inward-facing conformational states, sparing the equivalent step(s) during the movement of the empty transport domain. These results reveal a hitherto unknown role for the 3L4 in modulating an essential step in the transport process.

INTRODUCTION

Glutamate is the major excitatory neurotransmitter in the mammalian central nervous system, mediating synaptic transmission by activating receptors in post-synaptic neurons (1). Glutamate is removed by reuptake into glia and neurons by members of the EAAT family,

which transport 1 glutamate molecule into the cell coupled to 3 Na^+ ions and 1 H^+ accompanied by the countertransport of 1 K^+ ion (2). EAATs are members of the dicarboxylate/amino acid:cation symporter (DAACS) family (TCDB ID 2.A.23) that also includes members that transport dicarboxylates and other amino acids (3-5). Glt_{Ph}, from the archaeon *Pyrococcus horikoshii*, is 30% identical to the EAATs (6), and transports aspartate (L-asp); it is the only DAACS member for which there is high resolution structural information (7-10). Glt_{Ph} is an excellent model for the EAATs with similar functional properties, including the co-transport of substrate with 3 Na^+ ions (11,12) and the presence of a thermodynamically uncoupled anion conductance (13). However, Glt_{Ph} does not require K^+ to recycle the glutamate-free transporter from inward facing to outward facing states, instead recycling in a substrate- and ion-free state (11).

Glt_{Ph}, like other members of the EAAT family, is a trimer; each protomer consists of 8 transmembrane helices (TMs) and 2 re-entrant hairpin loops – the tips of which, along with transmembrane helices 7 and 8, form the substrate binding site (7,14) (Fig. 1A). Each protomer is organized into 2 distinct domains; a stationary trimerization domain that mediates all intersubunit contacts, and a mobile transport domain that fully encompasses the substrate binding site (9,15). Crosslinking, structural, computational studies, and more recently, electron paramagnetic resonance (EPR) spectroscopy suggest a model in which the transport domain moves ~18 Å and rotates ~30° through the trimerization domain (9,16-18). In a simple kinetic scheme for Glt_{Ph}, L-asp and 3 Na^+ ions bind to the outward facing state (OFS) (Fig. 1B, step 1), facilitating this dramatic conformational change and resulting in a piston-like movement of the substrate binding site across the membrane (Fig. 1B, step 2); in our scheme this step includes the formation of an occluded outward facing state ("closing", perhaps by HP2 closure), the large scale translocation of the domain, and the transition from "inward occluded" to "inward open" substrate-bound states ("opening"). The substrates are released into the cytoplasm from this inward facing state (IFS) (Fig. 1B, step 3) and the empty transport domain transitions from the IFS back to OFS to restart the cycle (Fig. 1B, step 4; note that in the mammalian isoforms K^+ is bound for this step). This return step also presumably includes "closing" and "opening" steps to permit the translocation step of the occluded *apo* transporter (whose structure was recently published (19)).

The trimerization domain is attached to the transport domain by 3 loops connecting TMs 2-3, 3-4 (3L4) and 5-6 (7). Comparison of the outward-facing and inward-facing crystal structures reveals distinct conformational changes in 2-3 and 5-6 loops; however, 3L4 was either unresolved or involved in lattice-packing interactions, meaning that the true structure of 3L4 is unknown (7,9). The 21 amino acid, proline-rich 3L4 undergoes substrate-dependent conformational changes, as demonstrated by limited trypsin proteolysis analysis and fluoroscein-5-maleimide accessibility experiments (20). Furthermore, cleaving the protein backbone within 3L4, by means of an engineered Factor X protease recognition site, resulted in almost complete loss of transport activity despite the protein maintaining its structural integrity (20). This novel observation revealed that 3L4 plays a critical role in the transport cycle.

In this work, we probe the role of 3L4 in the mechanism of L-asp transport by Glt_{Ph} using crosslinking, binding, and transport assays. We demonstrate that cleaving 3L4 specifically inhibits one of the components of the translocation step of the substrate-loaded transport domain of Glt_{Ph} while sparing the equivalent component of the translocation of the substrate-free *apo* translocation domain, a conclusion with important implications for the overall mechanism of transport.

Experimental procedures

Protein expression and purification

All mutations were made using the Quikchange II site-directed mutagenesis kit (Agilent Technologies) and all cysteine substitutions were introduced into a cys-less Glt_{Ph} mutant wherein the single native cysteine had been mutated to serine (C321S), which is fully active (20). Purification of wild-type Glt_{Ph} and its variants was performed essentially as described

previously (11). A culture of *E. coli* TOP10 cells harboring the appropriate expression vector was grown to mid-log phase and expression was induced by addition of 0.1 % (w/v) L-arabinose. Cells were lysed by sonication and membranes were isolated by multiple centrifugation steps. Membranes containing overexpressed, his-tagged protein were solubilized by addition of *n*-dodecyl *B*-D-maltopyranoside (DDM, Anatrace) and incubated for 1 hour at 4°C with Ni-NTA Superflow resin (Qiagen) pre-equilibrated with buffer containing 20 mM Tris HCl, pH 7.4, 200 mM NaCl, 5 mM L-glutamate, 0.5 mM TCEP and 2 mM DDM. Contaminants were removed by washing with 20 column volumes (CV) of the same buffer plus 40 mM imidazole. Bound protein was eluted by addition of the same buffer plus 250 mM imidazole. The his-tag was removed by overnight, room temperature incubation with thrombin in a ratio of 10 U/mg protein. Thrombin digestion was quenched by addition of 10 mM EDTA and 1 mM AEBSF.

Protein reconstitution

Reconstitution of Glt_{Ph} was achieved using the process pioneered by Rigaud and coworkers (21). Pre-formed liposomes were partially solubilized with Triton X100 (TX100), protein was added resulting in comicellization of the constituents, and detergent was removed using polystyrene beads (Biobeads SM-2). After obtaining inconsistent transport rates, we thoroughly examined the variables involved and found that to obtain high activity proteoliposomes we needed to a) add TX100 from a 10% (w/v) solution of instead of adding from the 100% detergent stock and b) use the light scattering curve to determine the correct detergent ratio for each batch reconstitution rather than using a fixed, predetermined TX100:lipid ratio. A 3:1 ratio of *E. coli* polar lipid extract and 1-palitoyl-2-oleoyl-sn-glycero-3-phosphocholine (POPC, Avanti Polar Lipids) are mixed, dried, and resuspended to 10 mg/ml in Inside Buffer (20 mM Tris/HEPES, pH 7.4, 1 mM NaCl and 199 mM KCl), unless indicated otherwise. The lipid suspension was freeze-thawed 5 times, extruded and then diluted to 4 mg/ml. Aliquots of 10% TX100 were added to the liposomes and incorporation was monitored using absorbance at 540 nm. Upon saturation of the liposomes with TX100, purified protein was added in a ratio of 3 µg protein/mg lipid. Detergent was removed by multiple additions of Biobeads SM-2 polystyrene beads (Bio-rad). Liposomes were separated from Biobeads and collected by ultracentrifugation. Proteoliposomes were resuspended in Inside Buffer to a final concentration of 10 mg/ml (lipid content), snap frozen and stored at -80°C.

Transport assays

Proteoliposomes were thawed, extruded through a 400 nm filter, collected by ultracentrifugation and resuspended to a final lipid concentration of 100 mg/ml. In a standard transport assay, the reaction was initiated by diluting proteoliposomes 150-fold into reaction buffer containing 20 mM Tris/HEPES, pH 7.4, 100 mM KCl, 100 mM NaCl, 1 µM valinomycin and 100 nM [^{3}H]-L-asp at 30°C. 200 µl samples were taken periodically and quenched by addition of 2 ml ice-cold quench buffer containing 20 mM Tris/HEPES, pH 7.4, 200 mM LiCl. The quenched reaction was applied to a nitrocellulose filter (Millipore) over a vacuum manifold and then washed with 2 ml of quench buffer. The nitrocellulose filters were dissolved with 3 ml FilterCount liquid scintillation cocktail (PerkinElmer) and radioactivity was counted using Trilux beta counter (PerkinElmer). The solute counterflow assay was performed in the same way except the proteoliposomes were loaded with buffer containing 20 mM Tris/HEPES, pH 7.4, 100 mM NaCl and 1 mM L-asp by multiple freeze/thaw cycles and extrusion through 400 nm filter. The reaction buffer contained 20 mM Tris/HEPES, pH 7.4, 100 mM NaCl and 100 nM [^{3}H]-L-asp.

Factor X digestion

Purified Glt_{Ph} variants were exchanged into Factor Xa digestion buffer (10 mM Tris/HEPES, pH 8, 5 mM $CaCl_2$, 100 mM NaCl and 2 mM DDM). Factor X (New England Biolabs) was added in a ratio of 125 µg/1 mg protein and incubated at 37°C for 24 hours. To discourage the stabilization of the IFS by disulfide formation between 55C and 364C during the 24 hour incubation, where applicable, we added 1 mM L-asp to the reaction. Factor X digestion

was stopped by addition of 10 mM EDTA and 1 mM AEBSF. Control samples that were not digested with Factor X were treated in an identical fashion.

Filter binding assays

Following purification by immobilized metal affinity chromatography and digestion by Factor X (both described previously), Glt_{Ph}Xa was further purified and exchanged into binding buffer (20 mM Tris/HEPES, pH 7.4, 200 mM choline chloride, 10 mM NaCl, 1 mM DDM) using size exclusion chromatography (Superdex 200 10/300 GL). 0.2 μM protein was incubated with a range of [^{3}H]-L-asp concentrations (made up in the same buffer) for 2 hours at room temperature. Binding was quenched and protein was precipitated by addition of ice-cold 50% ammonium sulfate. Precipitated protein was applied to a nitrocellulose filter over a vacuum manifold and washed with 2 ml 50% ammonium sulfate. The filters were dissolved in 3 ml FilterCount liquid scintillation cocktail (PerkinElmer) and radioactivity was counted using Trilix beta counter (PerkinElmer). Background binding of radiolabelled substrate was measured by performing the same experiment in the absence of protein. Binding curves are fit to a single site saturation model;

$$y = \frac{B_{max}X}{K_d + X}$$

Chemical crosslinking

Protein was crosslinked with 1,1-Methanediyl Bismethanethiosulfonate (MTS-1-MTS, Toronto Research Chemicals) by first exchanging the protein into buffer containing 20 mM Tris/HEPES, pH 7.4, 5 mM EDTA and 2 mM DDM and then, unless stated otherwise, incubating a 10 μM protein solution with 50 μM crosslinker (dissolved DMSO). Uncrosslinked controls were treated in the same way, but with an equivalent volume of DMSO instead of MTS-1-MTS. The crosslinking reaction was incubated at 37^{o}C for 30 minutes and quenched by addition of 100 mM *S*-Methyl methanethiosulfonate (MMTS, Sigma Aldrich). The crosslinking timecourses were performed at room temperature. Crosslinking timecourse data was fit to a single exponential model described by the following;

$$Y = Y_0 + a(1 - e^{-kx})$$

where, Y_0 is the Y value at time zero, a is the amplitude of the curve, k is the rate constant.

We first set out to explore the effects of 3L4 cleavage on protein conformational sampling by using Hg^{2+}-based crosslinking; a well-established method used successfully with Glt_{Ph} (8,9,22). However, not only are false positives an issue with Hg^{2+} crosslinking, wherein Hg^{2+}-induced protein band shifts are observed when no crosslink is formed (8), but it is also difficult to quench the Hg^{2+} crosslinking reaction with commonly used quenching compounds, such as *N*-ethyl maleimide (NEM) or *S*-methyl methanethiosulfonate (MMTS). In the absence of a quenching reagent, when attempting to crosslink cleaved Glt_{Ph} in detergent solution, we observed protein bands on SDS-PAGE gels corresponding to crosslink formation between intra-protein fragments and also, surprisingly, inter-subunit fragments. We reasoned unwanted crosslinking was occurring between unreacted cysteines and residual Hg^{2+} ions in the quasi-denatured environment of the SDS-PAGE gel or sample buffer. This led to difficulties in differentiating genuine intramolecular crosslink products from intact protein and crosslinking artifacts. We therefore switched to using the homobifunctional thiol-reactive reagent, 1,1-Methanediyl Bismethanethiosulfonate (MTS-1-MTS, linker length ~5 Å), which we could effectively and rapidly quench with an excess of MMTS. Indeed, pre-treatment of detergent-solubilized Glt_{Ph}XaC2 with MMTS prevented any crosslinking from taking place between 55C and 364C even in intact protein.

Densitometry

Densitometric SDS-PAGE band analysis was performed using Alphaview software (Cell Biosciences). Each protein band was selected using identically sized boxes and background values were obtained by selecting an identically sized box from a blank region of the gel directly below the band. Values were normalized to a control protein band of known amount.

RESULTS

Cleaving 3L4 does not prevent Glt_{Ph} from sampling the inward-facing conformation

The observed reduction in transport activity by Glt_{Ph} cleaved at residue 125 in the 3L4 may be due to a decrease in the protein's ability to sample particular states in the transport cycle, to changes in its ability to bind substrate or Na^+, to changes in transition rates between two or more cycle states, or a combination thereof. We sought here to distinguish among these possibilities.

The transition of the Glt_{Ph} transport domain between the outward- and inward-facing conformations is a major conformational rearrangement required for alternating access in this protein (9). To determine whether cleaving 3L4 restricts Glt_{Ph}'s access to one key state, the IFS, we introduced cysteines at positions known to form crosslinks only in that state (9). If such crosslinks form effectively after cleaving 3L4, Glt_{Ph} must be able to sample the inward-facing conformation despite loop scission. Using a gel-based crosslinking assay, we monitored IFS formation in purified, detergent-solubilized, Glt_{Ph} by introducing cysteines at positions 55 and 364 into a cys-less background with a Factor X site at residue 125 (from now on referred to as Glt_{Ph}XaC2, Fig. 1A). Cysteines in these positions were first shown to form a disulfide bond during an electrophysiological characterization of EAAT1 (23). Subsequently, an x-ray structure of the crosslinked form of the equivalent Glt_{Ph} mutant showed that cysteines in these positions are only in close proximity in the IFS (IFS Cα-Cα distance = 7.3 Å, OFS Cα-Cα distance = 27.6 Å) (9). Furthermore, stabilizing the IFS of Glt_{Ph} by crosslinking residues 55 and 364 increases the protein's electrophoretic mobility, making it easily discernible from non-crosslinked protein on a polyacrylamide gel (9). Here, crosslinking was performed in the absence of substrate, so the inward-facing state stabilized will be predominantly empty transporter (Fig. 1B, black box). Initial attempts to crosslink cleaved Glt_{Ph}XaC2 with Hg^{2+} were complicated by extraneous reactions with the metal (see *Experimental Procedures*), so we developed an alternative approach based on the homobifunctional thiol-reactive reagent, 1,1-Methanediyl Bismethanethiosulfonate (MTS-1-MTS, linker length ~5 Å).

In the absence of Factor X treatment, the predominant protein band is full length (FL), non-crosslinked Glt_{Ph}XaC2 (Fig. 1C, Lane 1). A small population of crosslinked protein was also apparent, caused by oxidative disulfide formation during the 24 hour incubation, a fact confirmed by the disappearance of this band after reduction with β-mercaptoethanol (β-ME) (Fig. 1C, lane 2). Treatment of Glt_{Ph}XaC2 with Factor X produced two fragments (NTF, N-terminal fragment and CTF, C-terminal fragment) with no full length protein remaining (Fig. 1C, lane 3). Minimal changes in electrophoretic migration of the two fragments upon reduction with β-ME indicate that the protein band positions are not caused by aberrant crosslinking events (Fig. 1C, lane 4). We observed small, crosslink independent differences in all protein band migration profiles in the presence of β-ME. Treating detergent-solubilized Glt_{Ph}XaC2 with MTS-1-MTS alone led to increased electrophoretic mobility, indicative of IFS crosslink formation, and was fully reversible with β-ME treatment (Fig. 1C, lanes 5 and 6). Cleaving Glt_{Ph}XaC2 produces only NTF and CTF fragments, however, if the fully cleaved protein is then treated with MTS-1-MTS, a third, higher molecular weight protein band was also apparent, which is the product of crosslinking the N- and C-terminal fragments (Fig. 1C, lane 7). We confirmed that this band is formed by crosslinking between the proteolytic fragments because, upon reduction, we observed disappearance of the high molecular weight band and an intensification of the N- and C-terminal fragments (Fig. 1C, lane 8). Mutants containing the Factor X site and the single cysteine substitutions did not form this crosslinked band, indicating that both cysteines in the engineered crosslinking pair are required and that intermolecular crosslinking is not responsible (data not shown). This result demonstrates that, despite lacking an intact 3L4, Glt_{Ph} is still able to sample the inward-facing conformation in detergent solution.

In a related assay, where Glt_{Ph}XaC2 is first locked into the IFS by treatment with MTS-1-MTS and then digested with Factor X, we observe full cleavage of 3L4, indicating that 3L4

is accessible to protease in the inward-facing conformation (data not shown).

To complement this work, we also made several attempts to stabilize the OFS using engineered cysteines; K55C-G280C, V51C-T275C, L212C-V274C, V216C-A391C, Q220C-I389C, V58C-P283C and L66C-S300C. For all pairs attempted, the introduced cysteine pairs either did not crosslink using MTS-1-MTS (however, one of these examples, L66C-S300C, does crosslink robustly with Hg^{2+}; its structure has been published recently (22)) or a disulfide would form during purification despite efforts to prevent it. These disulfide bonds could only be reduced under harsh conditions that would render the protein inactive.

Cleaved Glt_{Ph} has Na^+-driven L-asp transport activity

Having demonstrated that cleaving 3L4 does not prevent Glt_{Ph} from accessing at least one conformation essential to the transport cycle, we reassessed the transport capabilities of cleaved Glt_{Ph}. Following incubation of purified wildtype Glt_{Ph} (Glt_{Ph}WT) and Glt_{Ph}Xa (Glt_{Ph} containing a Factor X recognition site at residue 125) in the presence and absence of Factor X, we reconstituted the treated proteins into liposomes using an optimized protocol (see *Experimental Procedures*). This protocol increased the substrate uptake approximately fivefold, and thereby permitted detection of transport activity in the Factor Xa cut GltPhXa, activity we could not detect with our previous methods (20). SDS-PAGE analysis of the proteins prior to reconstitution revealed that treatment of Glt_{Ph}Xa with Factor X resulted in complete digestion, whereas, under identical conditions, Glt_{Ph}WT remained intact (Fig. 2B). We monitored initial rates of ^{3}H-L-asp transport into proteoliposomes containing cleaved Glt_{Ph} in the presence of an inwardly-directed sodium gradient and, contrary to the negligible activity we previously reported, we observed reduced, but still easily detectable activity (~30% compared to wild-type). There were no apparent effects on the activity of Glt_{Ph}WT after treatment with Factor X (Fig. 2A). Uncut Glt_{Ph}Xa has lower activity (~70%) than Glt_{Ph}WT, which is likely due to the effects of the amino acid substitutions in 3L4 required to introduce the Factor X recognition site and, as demonstrated by the SDS-PAGE analysis, not from cleavage of the protein during expression and purification (Fig. 2B).

The ability to support the transport of L-asp, albeit with decreased efficacy, clearly demonstrates that even with a fully cleaved 3L4, Glt_{Ph} can sample all the conformations necessary for transport. The reduced transport rates must therefore stem from either altered thermodynamic properties of one or more states in the cycle or from altered kinetic properties of one or more transitions in the cycle. We sought to establish which part of the transport cycle is compromised upon 3L4 cleavage by systematically isolating steps and transitions of the cycle and observing the impact of 3L4 cleavage at each stage.

Cleavage of 3L4 minimally affects substrate interaction

Closure of HP2, the outer hairpin, is thought to be an essential step in forming the Glt_{Ph} substrate binding site and allowing translocation of the transport domain. Given that 3L4 directly overlies the HP2 hairpin, we considered the possibility that the loop stabilizes the open state of the hairpin, thereby influencing substrate and Na^+ binding (7,9). If true, this hypothesis predicts that cleavage of 3L4 would substantially affect substrate binding. We tested this model by deriving the kinetic parameters of transport (V_{max} and K_m, see Table 1) using functional protein reconstituted into lipid vesicles. The L-asp dose response reveals a modest decrease in the K_m of cleaved protein (69.5 ± 14.1 nM compared to 129.5 ± 16.8 nM for Glt_{Ph}WT, Fig. 3A and Table 1), and a large decrease in the V_{max} (9.2 ± 0.7 nmol/mg/min compared to 42.7 ± 4.5 nmol/mg/min for Glt_{Ph}WT, Fig. 3A and Table 1). We observed the same effects of cleaving 3L4 on the Na^+-dependence of transport: minimal difference to the K_m values and a large decrease in the V_{max} (Fig. 3B). As expected, treatment with Factor X had no effect on the K_m or V_{max} values for either L-asp or Na^+ of Glt_{Ph}WT (Fig. 3A and B and Table 1). Glt_{Ph}Xa, in the absence of Factor X treatment exhibits a lower K_m compared to wild-type; this is likely due to the 4 amino acid substitution made to create the Factor X site in 3L4 (Table 1 and (20)).

These data reveal that cleaving 3L4 does not substantially affect the K_m of Glt_{Ph} for either L-asp or Na^+. If 3L4 cleavage had a major impact on substrate binding, K_D, we would expect this to be reflected in the K_m. The preservation of K_m therefore indicates that the substrate binding/unbinding events during the transport cycle are at most minimally affected by 3L4 scission (Fig. 3B, *inset*, steps 1 and 3).

To corroborate this data, we directly measured the binding of L-asp to detergent solubilized protein and calculated the dissociation constants (K_D) for cleaved and intact Glt_{Ph}Xa. Attempts were made to assess L-asp binding using both isothermal titration calorimetry (ITC), a technique recently used to great effect with Glt_{Ph} (22), and equilibrium dialysis. Both methods proved unsuitable for different, technical reasons; the former, due to the large amount of cleaved protein required (the amount of Factor X protease required being the limiting factor) and the latter, due to the inconsistent data presumably caused by the substrate interacting with the dialysis membrane. Ultimately, data obtained using a filter binding assay revealed robust aspartate binding by both intact and cleaved Glt_{Ph}Xa (Fig. 3C). We observed no substantial difference in the K_D between intact and cleaved protein (4.0 ± 0.1 μM and 1.4 ± 0.3 μM, respectively) indicating that substrate binding is essentially preserved after 3L4 loop scission. Using this method, we measure a K_D of 1.0 ± 0.3 μM for Glt_{Ph}WT (a value in good agreement with the Glt_{Ph}WT K_D obtained using ITC under similar conditions (22)) revealing that introduction of the Factor X site into the 3L4 loop of Glt_{Ph} results in a slight decrease in affinity, a decrease that is reversed upon cleavage of the loop (Fig. 3C and Table 1).

Thus, the observed decrease in transport activity is not a consequence of decreased affinity of binding rate, but is due to a lower transport turnover rate, highlighting the possibility that cleaving 3L4 impedes other steps in the transport cycle.

The activation energy of transport is increased when 3L4 is cleaved

The activation energy, E_a, of a process reflects the relative height of the energetic barrier that must be hurdled for that process to occur. If the effects of 3L4 cleavage are due to alterations in a significant energy barrier in one of the rate-limiting transport cycle reactions, then we would expect cleavage to cause changes in the E_a of transport. These changes, in turn, should be reflected in the temperature-dependence of transport.

Over a temperature range of 3-40°C, we observed a ~16 and ~64-fold increase in the initial rates of ^{3}H-L-asp transport by intact and cleaved Glt_{Ph}Xa, respectively (Fig. 4A). Analyses of these data with an Arrhenius plot revealed a clear temperature dependence for the transport rate and corresponds to an E_a of 56.6 kJ.mol^{-1} and a temperature coefficient (Q_{10}) of 2.13 for intact Glt_{Ph}Xa (Fig. 4B). The Q_{10} value and E_a for cleaved Glt_{Ph}Xa are ~1.5-fold higher than intact mutant (3.1 and 83.7 kJ.mol^{-1}, respectively) indicating a higher energy barrier to at least one step in the transport cycle. The activation energy values are composites of the temperature dependence of various conformational transition rates during the transport cycle, but combined with our evidence that the binding reactions are minimally affected by 3L4 cleavage these data point to other steps in the cycle, namely the closing/opening and translocation reactions of loaded and unloaded transport domains. Since our current experimental methods do not have the resolution to distinguish among these steps, we will henceforth collectively refer to them as the "transfer steps" since together they transfer the accessible substrate binding sites from one face of the membrane to the other. These steps together comprise step 2 (the *loaded* transfer) for the substrate-loaded transporter and step 4 (the *apo* transfer) for the empty protein in our simplified kinetic scheme (Figure 1B).

Cleaving 3L4 results in severely diminished substrate exchange

Thus, the transfer reactions are groups of conformational changes that alternately expose the substrate binding site from one side of the membrane to the other; the loaded transfer step can be isolated from net transport by monitoring protein-facilitated *exchange* of substrate across the membrane. In an exchange experiment, equimolar concentrations of Na^+ and L-asp are introduced on either side of the membrane, then

substrate is exchanged between the external and internal solutions at equilibrium as the substrate binding site stochastically samples both sides of the membrane (24). By spiking the external solution with ^{3}H-L-asp, exchange is measured by monitoring ^{3}H-L-asp accumulation in the lumen of the proteoliposome. Despite several efforts to apply this method to Glt_{Ph}-containing proteoliposomes, we could not measure appreciable radiolabel accumulation. However, we overcame this problem using a solute counterflow assay; here, proteoliposomes are loaded with excess unlabeled substrate (1 mM) and diluted into an external solution containing a trace amount of radiolabeled substrate (100 nM). Here, as in exchange mode, the alternating exposure of the substrate binding site to both sides of the membrane will initially result in exchange of unlabeled substrate in the proteoliposome lumen for radiolabeled substrate in the external solution (Fig. 5, *inset*, steps 1, 2 and 3). In counterflow, however, the relative concentration of radiolabeled and unlabeled substrate in the proteoliposome lumen essentially eliminates the likelihood of the accumulated radiolabeled substrate from rebinding and exiting back into the external solution. At first, this results in uptake of radiolabel by a process identical to exchange. Eventually, however, the accumulation of radiolabel in the proteoliposome lumen peaks and the accumulated substrate effluxes from the proteoliposomes until the outwardly directed substrate gradient is dissipated (25). If the turnover rate of the transporter is slow, as it is for Glt_{Ph}, then substrate exchange can be monitored separately from the efflux portion of counterflow.

Under these experimental conditions, we observe robust accumulation of ^{3}H-L-asp in proteoliposomes containing Glt_{Ph}WT or intact Glt_{Ph}Xa as a function of time (Fig. 5). In contrast, we observed very slow accumulation of ^{3}H-L-asp in proteoliposomes containing cleaved Glt_{Ph}Xa: ~8-fold lower accumulation after 10 minutes compared to proteoliposomes containing intact Glt_{Ph}Xa (Fig. 5). Note that we do not continue these experiments long enough to observe the falling phase of the counterflow reaction. This experiment isolates substrate binding/unbinding events (Fig. 5, *inset*, steps 1 and 3) and the transition of the substrate-loaded transport domain (Fig. 5, *inset*, step 2) from the rest of the transport cycle. Having already demonstrated that 3L4 cleavage causes minimal perturbation of substrate interaction, this result shows that loop scission substantially attenuates the substrate-loaded transfer reaction.

Efficient transition between substrate-loaded OFS and IFS depends on an intact 3L4

The counterflow experiments implicate 3L4 in the loaded transfer reaction but provide no information on whether 3L4 scission affects the equivalent transition of the apo, substrate-free transport domain (Fig. 5, *inset,* step 4). We therefore sought to compare the effects of loop scission on the transfer of the empty transport domain, with those of the cleavage on the fully loaded form. Since transport measurements will not report on isolated transitions of substrate-free forms of the protein, we measured the effects of loop cleavage on the empty (Fig. 6C, left panel, step 4) and substrate-loaded (Fig. 6C, right panel, step 2) equilibria separately by monitoring the rate of IFS crosslink formation in the absence or presence of saturating substrate concentration, respectively. If the energetics of the transfer reactions are affected then the population of the crosslink-competent, inward-facing state will be altered and will be reflected as a change in the crosslinking rate.

We quantified the rate of IFS crosslink formation of cleaved and intact Glt_{Ph}Xa in the presence and absence of substrate using SDS-PAGE and densitometric analysis (Fig. 6A and B). IFS crosslink formation was determined for both intact and cleaved protein by quantifying the intensity of the crosslinked band (labeled "CL" in Fig. 6A). For intact protein, the crosslinked band is reflected in a shift of the full length protein band toward faster electrophoretic migration; for cleaved protein, a single crosslinked band is formed by the crosslinking of the 2 proteolytic fragments (e.g. Fig. 1C, lane 7). In the absence of substrate, we observed rapid crosslink formation for both intact and cleaved protein. Cleaved protein crosslinks with a slightly faster rate than intact protein (rate constants of 1.4 and 0.78 min^{-1}, respectively) although it reaches a lower absolute level of crosslinking (75% compared to ~100% for intact

protein, Fig. 6A and B, left panel). Under these conditions, we predominantly monitored crosslink formation of empty transporter in equilibrium between the OFS and IFS (Fig. 6C, left panel, black box). These results suggest that cleaving 3L4 has little effect on the equilibrium of empty Glt_{Ph} between IFS and OFS (the *apo* transfer reaction, Fig. 6C, left panel, step 4). This observation is strikingly different from the crosslinking behavior in the presence of saturating concentrations of both substrates. Here, though the rate of IFS crosslink formation for intact Glt_{Ph} was similar to the crosslinking rate without substrate (0.81 min^{-1}), the crosslinking is slowed to an immeasurable rate in the cleaved protein, with no more than 3% crosslinking over the 10-minute course of the experiment. (Fig. 6A and B, right panel). These results indicate that cleaving 3L4 results in lower occupancy in the crosslink-competent, inward-facing conformation when in the presence of substrate than in the *apo* form of the protein. The greatly diminished crosslinking rate for cleaved Glt_{Ph} demonstrates that loop scission specifically impedes the substrate-loaded transport domain from accessing the crosslink-competent IFS (Fig. 6C, right panel, step 2).

Curiously, during this experiment we observed that crosslinking of intact protein in the presence of substrate (Fig. 6B, left panel, closed squares) does not reach completion. This result suggests that the presence of substrate prevents a population of the Glt_{Ph} (40%) from accessing the inward-facing, crosslink competent state; an unexpected result considering the irreversible nature of the crosslinking reaction. An alternative hypothesis is that the presence of substrate may make one or both of the cysteine residues more accessible to reaction with the crosslinking reagent. If this is the case, and if the rate of this reaction exceeds the rate of entry into the crosslink-competent state (OFS-IFS transition), each cysteine (C55 and C364) may react with different MTS-1-MTS molecules, thus preventing crosslink formation between the two cysteines via a single MTS-1-MTS molecule. We investigated whether this was the case by measuring crosslinking rates under conditions that would slow down the rate of the MTS reaction while leaving the rate of conformational change unaffected. Two parameters were varied that might result in the separation of these two events; concentration of MTS-1-MTS, and the pH of the reaction. In the absence of substrate, decreasing the concentration of crosslinker results in decreased rate of crosslink formation, but the absolute amount of crosslink formation remains essentially the same (Fig. 7A). In the presence of substrate, decreased crosslinker concentration also results in a lower crosslinking rate; however, the absolute amount of crosslinking is greater when lower concentrations are used (Fig. 7B). This demonstrates that when the crosslinking rate is slower, more crosslinking can occur, which we interpret to be due to the protein accessing the crosslink-competent state before the cysteines react with one MTS-1-MTS each.

MTS reagents react predominantly with the ionized thiolate form of cysteine which is more abundant at higher pHs, therefore decreasing the pH of the reaction should decrease the rate of crosslinking. Conveniently, the transport rate of Glt_{Ph} remains constant over a wide range of pHs indicating that transport, and any associated conformational shift, is insensitive to pH change (11). Crosslinking timecourses were performed in the presence and absence of substrate at pH 5, 7 or 9. In the absence of substrate, decreasing the pH of the reaction decreased the rate of crosslinking, however the absolute amount of crosslinking was the same regardless of the pH (data not shown). In the presence of substrate, decreasing the pH resulted in a lower crosslinking rate, but resulted in a higher absolute amount of crosslinking compared to the crosslinking performed at higher pHs (data not shown). Together, these findings strongly suggest that the incomplete crosslinking we observe in our experiments is due to reactions of the two cysteines with separate MTS-1-MTS molecules. This phenomenon results in competition between the reaction of interest, crosslinking the cysteines together with one MTS-1-MTS molecule, and a side reaction, where each exposed cysteine reacts with a separate MTS-1-MTS molecule, preventing crosslink formation. However, the crosslinking rates themselves, which are the measurement of interest, are not compromised by the side reaction.

DISCUSSION

Here, we explored the mechanism by which the 3L4 influences the transport cycle in Glt_{Ph}, using a combination of 3L4 proteolytic cleavage, chemical crosslinking, and transport measurements to specifically probe major components of the transport cycle, distinguishing substrate binding, loaded transfer, and *apo* transfer reactions. In the context of a simplified kinetic scheme, which nonetheless captures the essential features of transport, we find strong evidence that the basic binding/unbinding reactions with substrate and Na^+ are minimally affected by cutting 3L4, and, surprisingly, that the transfer of the empty transport domain is also preserved. Indeed, our experiments point to the loaded transfer, which includes opening and closing steps and the major translocation of the fully loaded and occluded transport domain across the membrane as the locus affected by cutting 3L4, primarily through effects on the activation energy of translocation. This finding implies that the structure of the unloaded transport domain is significantly different from that of the loaded domain, an idea strongly supported by a recent structure of an *apo* form of a Glt_{Ph} homolog (19).

The simplified model we have focused on to this point (Fig. 1B) distinguishes steps that can be isolated using our functional experiments. Clearly though, each of these reactions comprises multiple substeps which we cannot identify functionally. By lumping the binding reactions of L-asp and Na^+ our kinetic scheme captures the general features of the binding portions of the transport cycle without requiring a specific binding order. Clearly, a more detailed model would include separate binding steps for L-asp and Na^+, ideally in a particular order (26), see Fig. 8 (beige reactions). But by working at zero or saturating substrate/Na^+ we can safely ignore these details.

As we have discussed, the transfer reaction must include multiple substates (8) as shown in the blue reactions in Fig. 8. The transfer steps in our model (Fig. 8, steps 2 and 4) each include three substeps: between outward-open and outward-occluded, between outward-occluded and inward-occluded (the piston movement), and between inward-occluded and inward-open as indicated in Fig. 8. At the level of our experiments, though, these detailed reactions would be difficult or impossible to isolate; our results do not distinguish which one (or more) of these substeps is affected by 3L4 cleavage in the substrate-loaded form of the transport domain. Our findings do, importantly, clearly and definitively distinguish between the behavior of the *apo* transport domain and the loaded domain for the *overall* transition that captures these three experimentally indistinguishable substeps, with only the loaded domain affected by 3L4 cleavage (Fig. 8, blue shading).

Due to the position of 3L4, directly overlying the HP2 hairpin, an attractive proposition for its role is to stabilize one or more states of the hairpin, thereby modulating the binding of protein to substrate. Since opening of HP2, as observed in the L-asp- and TBOA-bound structures, may bring it into more intimate contact with 3L4, we considered the possibility that 3L4 could be stabilizing that state, which would in turn affect the binding sites of both substrate and inhibitor. However, we eliminated this possibility after measuring the kinetic parameters for cleaved and intact Glt_{Ph} (Fig. 3). Measurements of both K_m and K_D suggest that 3L4 cleavage has minimal effects on the substrate binding rates and affinities. Our results therefore focus attention on the kinetic properties of the transfer reactions, showing that the activation energy barrier for one part of this reaction is raised by 3L4 cleavage.

The strong temperature dependence of active transport reflects all the temperature dependent reactions that occur during the transport process, including substrate binding and conformational changes. In the Glt_{Ph} homolog EAAC1, the binding of substrate is associated with a low energy of activation and is diffusion controlled; binding of substrate and any associated conformational changes do not significantly contribute to the temperature dependence of transport (27). Additionally, the K_m of wild type Glt_{Ph} for Na^+ is stable between 30°C and 40°C despite a large difference in the maximum transport rate (11). Together, these results suggest, at least for Na^+, that the substrate binding event for Glt_{Ph} is relatively temperature independent and support the conclusion that the

difference in the temperature dependence between cleaved and intact Glt_{Ph}Xa primarily reflect the isolated transfer reactions.

What is the structural basis of transport modulation by 3L4? Cysteine-scanning mutagenesis of 3L4 revealed that many single amino acid substitutions result in altered transport activities (17), hinting that specific interactions between residues in 3L4 and another part of the protein are important for transport. Results reported here suggest a model in which the intact 3L4 interacts specifically with the loaded transport domain, thereby stabilizing a specific transition state in the translocation process (Fig. 8), a model supported by the protection of the loop from proteolysis in the presence of substrate (20). We speculate, based on the location of 3L4, that this stabilization might be mediated by interactions between 3L4 and HP2, which directly underlies the loop in the OFS structure. In order for 3L4 to discriminate between substrate-loaded and empty transport domain, as is demonstrated by our data, the transport domain must have an appreciably different form in the presence and absence of substrate. This hypothesis is supported by a newly published structure of a Glt_{Ph} homolog in the *apo* form which shows subtle but clear changes in the disposition of HP2 (19). This implies a kind of asymmetry in the transport cycle, with the structure of the translocating unloaded domain detectably (to 3L4) different from that of the loaded domain, a possibility not captured in previous models of transport, which assume similar "closed" forms of the protein for both translocation steps (e.g. steps 2 and 4 in Fig. 1B). These observations offer the possibility of additional protein conformations in these transporters that might serve as targets for state-specific, or subtype specific drugs to modulate their function.

ACKNOWLEDGEMENTS

We thank Kenton Swartz and Jeff Diamond for critical reading of the manuscript. This work was supported by the Intramural Research Program of the NIH, NINDS.

REFERENCES

1. Danbolt, N. C. (2001) *Progress in neurobiology* **65**, 1-105
2. Zerangue, N., and Kavanaugh, M. P. (1996) *Nature* **383**, 634-637
3. Saier, M. H., Jr., Tran, C. V., and Barabote, R. D. (2006) *Nucleic acids research* **34**, D181-186
4. Arriza, J. L., Kavanaugh, M. P., Fairman, W. A., Wu, Y. N., Murdoch, G. H., North, R. A., and Amara, S. G. (1993) *The Journal of biological chemistry* **268**, 15329-15332
5. Groeneveld, M., Weme, R. G., Duurkens, R. H., and Slotboom, D. J. (2010) *Journal of bacteriology* **192**, 2900-2907
6. Slotboom, D. J., Konings, W. N., and Lolkema, J. S. (1999) *Microbiol Mol Biol Rev* **63**, 293-307
7. Yernool, D., Boudker, O., Jin, Y., and Gouaux, E. (2004) *Nature* **431**, 811-818
8. Verdon, G., and Boudker, O. (2012) *Nature structural & molecular biology* **19**, 355-357
9. Reyes, N., Ginter, C., and Boudker, O. (2009) *Nature* **462**, 880-885
10. Boudker, O., Ryan, R. M., Yernool, D., Shimamoto, K., and Gouaux, E. (2007) *Nature* **445**, 387-393
11. Ryan, R. M., Compton, E. L., and Mindell, J. A. (2009) *The Journal of biological chemistry* **284**, 17540-17548
12. Groeneveld, M., and Slotboom, D. J. (2010) *Biochemistry* **49**, 3511-3513
13. Ryan, R. M., and Mindell, J. A. (2007) *Nature structural & molecular biology* **14**, 365-371
14. Yernool, D., Boudker, O., Folta-Stogniew, E., and Gouaux, E. (2003) *Biochemistry* **42**, 12981-12988
15. Groeneveld, M., and Slotboom, D. J. (2007) *Journal of molecular biology* **372**, 565-570
16. Crisman, T. J., Qu, S., Kanner, B. I., and Forrest, L. R. (2009) *Proc Natl Acad Sci U S A* **106**, 20752-20757

17. Georgieva, E. R., Borbat, P. P., Ginter, C., Freed, J. H., and Boudker, O. (2013) *Nature structural & molecular biology* **20**, 215-221
18. Hanelt, I., Wunnicke, D., Bordignon, E., Steinhoff, H. J., and Slotboom, D. J. (2013) *Nature structural & molecular biology* **20**, 210-214
19. Jensen, S., Guskov, A., Rempel, S., Hanelt, I., and Slotboom, D. J. (2013) *Nature structural & molecular biology* **20**, 1224-1226
20. Compton, E. L., Taylor, E. M., and Mindell, J. A. (2010) *Proceedings of the National Academy of Sciences of the United States of America* **107**, 12840-12845
21. Levy, D., Gulik, A., Bluzat, A., and Rigaud, J. L. (1992) *Biochimica et biophysica acta* **1107**, 283-298
22. Reyes, N., Oh, S., and Boudker, O. (2013) *Nature structural & molecular biology* **20**, 634-640
23. Ryan, R. M., Mitrovic, A. D., and Vandenberg, R. J. (2004) *J Biol Chem* **279**, 20742-20751
24. Lolkema, J. S., Carrasco, N., and Kaback, H. R. (1991) *Biochemistry* **30**, 1284-1290
25. Kaczorowski, G. J., and Kaback, H. R. (1979) *Biochemistry* **18**, 3691-3697
26. Kanner, B. I., and Bendahan, A. (1982) *Biochemistry* **21**, 6327-6330
27. Mim, C., Tao, Z., and Grewer, C. (2007) *Biochemistry* **46**, 9007-9018

FIGURE LEGENDS

Figure 1 Detergent-solubilized Glt_{Ph} can be trapped in the IFS when 3L4 is cleaved. (*A*) Structure of L-asp bound Glt_{Ph} ((7), PDB accession 1XFH) showing the K55C and A364C mutations (blue balls) in relation to HP1 (yellow), HP2 (red) and 3L4 (green). (*B*) Simple kinetic model of transport by Glt_{Ph}. Outward-facing transporter (T_O) binds Na^+ and L-asp (1), at which point the binding site transition across the membrane (2). Substrates are released from the inward-facing transporter (T_I) into the cytoplasm (3), and empty T_I transitions back to outward-facing. Black box signifies the state stabilized by the crosslinking reaction in (*C*). (*C*) SDS-PAGE gel showing the effects on the electrophoretic properties of Glt_{Ph}XaC2 after incubation at 37°C for 24hrs in the presence (+) and absence (-) of Factor X protease, followed by 20 min at 37°C in the presence (+) and absence (-) of crosslinking agent MTS-1-MTS. Samples were boiled in the SDS-PAGE sample buffer in the presence (+) and absence (-) of β-ME. Arrows indicate the positions of full length (FL) and crosslinked protein (CL), and the C-terminal (CTF) and N-terminal (NTF) fragment produced by Factor X proteolysis and/or chemical crosslinking.

Figure 2 Reconstituted Glt_{Ph} remains active after 3L4 cleavage. (*A*) Na^+-driven initial transport rates of ^{3}H-L-asp into proteoliposomes containing Glt_{Ph}WT and Glt_{Ph}Xa reconstituted after incubation at 37°C for 24 hours in the presence (+) and absence (-) of Factor X. Data is normalized to untreated Glt_{Ph}WT data and is the average of 3 datasets. Error bars indicate s.e.m. (*B*) Non-reducing SDS-PAGE gel of the treated protein reconstituted into the proteoliposomes used in (*A*). Arrows indicate the positions of Factor X (Fxa), full length protein (FL), and the proteolytic C-terminal (CTF) and N-terminal fragment (NTF).

Figure 3 Substrate dependence of transport and substrate binding activity of cleaved and intact Glt_{Ph}. Rate of ^{3}H-L-asp transport into proteoliposomes containing Glt_{Ph}WT (circles) and Glt_{Ph}Xa (squares) reconstituted after incubation at 37°C for 24 hours in the presence (open symbols) and absence (closed symbols) of Factor X as a function of (*A*) L-asp concentration or (*B*) Na^+ concentration in the external buffer. In (*A*), an inwardly-directed Na^+ gradient (1 mM [internal Na^+], 100 mM [external Na^+]) was applied for all samples. Data is fit to the Michaelis-Menton equation. In (*B*), 1 μM ^{3}H-L-asp was present in the external buffer. Data is fit to the Hill equation. The average of 3 datasets is shown throughout and error bars indicate s.e.m. Simple kinetic model for transport by Glt_{Ph} as in Fig. 1B is shown in the *inset*. Black symbols indicate states and steps of the model isolated in this experiment; light

gray symbols indicate steps not represented. Block arrows (white for cleaved, black for intact Glt_{Ph}) indicate effect of 3L4 cleavage on the steps isolated relative to intact Glt_{Ph}. This applies for all subsequent kinetic schemes shown. (*C*) Filter-based substrate binding assay showing amount of [^{3}H]-L-asp binding to 0.2 μM Glt_{Ph}WT (circles), 0.2 μM cleaved Glt_{Ph}Xa (open squares) and 0.6 μM intact Glt_{Ph}Xa (closed squares) as a function of substrate concentration. Data is fit with a one site saturation model. Reactions were performed in triplicate and error bars represent s.e.m.

Figure 4 Temperature dependence of transport by cleaved and intact Glt_{Ph}. (*A*) Effect of temperature on Na^+-driven transport of ^{3}H-L-asp into empty liposomes (closed diamonds), or proteoliposomes containing Glt_{Ph}Xa reconstituted after incubation at 37^{o}C for 24 hours in the presence (open squares) and absence (closed squares) of Factor X. The average of 4 datasets is shown and error bars indicate s.e.m. (*B*) Arrhenius plot of the Na^+-driven transport rate of ^{3}H-L-asp into proteoliposomes containing Glt_{Ph}Xa after incubation at 37^{o}C for 24 hours in the presence (open squares) and absence (closed squares) of Factor X as a function of temperature. The data is fit to a straight line.

Figure 5 Effects of cleaved 3L4 on the IFS-OFS transition (*A*) Rate of ^{3}H-L-asp accumulation in proteoliposomes containing Glt_{Ph}Xa reconstituted after incubation at 37^{o}C for 24 hours in the presence (open symbols) and absence (closed symbols) of Factor X. Counterflow assays were performed with lumenal buffer containing 1 mM L-asp and 100 mM NaCl and an external buffer containing 100 nM ^{3}H-L-asp and 100 mM NaCl. For comparison, data is shown for empty proteoliposomes (closed diamonds) and proteoliposomes reconstituted with Glt_{Ph}WT (closed circles). Data presented is the average of 4 datasets and error bars indicate s.e.m. Simple kinetic model for transport by Glt_{Ph} as in Fig. 1B is shown in the *inset*.

Figure 6 Effects of cleaving 3L4 on the rate of IFS crosslinking. MTS-1-MTS crosslinking timecourse of cleaved and intact Glt_{Ph}Xa in the absence (left panel) and presence of 1 mM L-asp and 100 mM NaCl (right panel). (*A*) Representative Coomassie-stained SDS-PAGE of crosslinking timecourse with intact (-FXa) and cleaved Glt_{Ph} (+FXa). Crosslinking was performed at room temperature. Arrows indicate position of full-length (FL) and crosslinked (CL) protein. (*B*) Densitometric analysis of relative amounts of crosslinked band in the presence and absence of substrate after treatment with (open symbols) and without (closed symbols) Factor X at each timepoint from (*A*). Analysis was performed using Alphaview software on a triplicate dataset. Error bars indicate s.e.m. Where possible, data was fit to a single exponential rise to maximum model. (*C*) Simple kinetic model for transport by Glt_{Ph} as in Fig. 1B.

Figure 7 Effects of crosslinker concentration on the rate and absolute amount of crosslinking. SDS-PAGE (left) and densitometric analysis (right) of the MTS-1-MTS crosslinking rate in the absence (A) and presence (B) of saturating substrate concentrations upon application of different concentrations of MTS-1-MTS. MTS-1-MTS was added to a solution containing 7 μM protein to make final crosslinker concentrations of 15 μM (green data), 25 μM (red) or 50 μM (black).

Figure 8 Model of transport modulation by 3L4. Cartoon model depicting conformational changes and predicted modulation of interaction between the transport domain (blue domain), the trimerization domain (grey domain), and 3L4 (black line). The simple model used to guide experimental interpretation is shown in pale colors (numbered as in previous figures), while a more detailed model, which includes essential reaction steps, is highlighted. Binding and unbinding of Na^+ (green circles) and substrate (magenta circle) occur in ordered steps in both inward and outward facing transporters (horizontal, beige reactions). '+' signs indicate that one or two Na^+ ions may bind in the indicated steps. Elements of the transfer reactions (vertical, blue reactions) include closing, translocation, and opening steps. Our results demonstrate that one or more reactions of the fully loaded transport domain (shaded blue) are affected by 3L4 cleavage suggesting that Na^+ and substrate binding induce conformational changes in the transport domain and

3L4, which result in altered interactions with 3L4, shown as a black line connecting the domains. HP1 (blue) and HP2 (red) are depicted in ‘open’ and ‘closed’ forms as appropriate.

Table 1

	L-asp dose response				Na^+ dose response		
	V_{max} (nmol mg^{-1} min^{-1})	K_m (nM)	K_{cat} (min^{-1})	K_d (μM)	V_{max} (nmol mg^{-1} min^{-1})	K_m (mM)	Hill coefficient
Glt_{Ph}WT	42.7 ± 4.5	129.5 ± 16.8	1.6	1.0 ± 0.3	35.4 ± 1.2	21.3 ± 13.5	2.3 ± 0.4
Glt_{Ph}WT + Fxa	31.7 ± 2.1	114.8 ± 12.8	1.2	-	36.3 ± 0.4	6.7 ± 0.5	3.0 ± 0.5
Glt_{Ph}Xa	60.6 ± 3.1	197.7 ± 7.8	2.2	4.0 ± 0.1	38.4 ± 3.7	11.8 ± 2.3	2.1 ± 0.3
Glt_{Ph}Xa + Fxa	9.2 ± 0.7	69.5 ± 14.1	0.3	1.4 ± 0.3	7.9 ± 0.5	10.6 ± 1	2.1 ± 0.2

Effects of cleaving 3L4 on the binding affinity kinetic parameters of transport. Kinetic parameters for cleaved and intact Glt_{Ph} were derived by fitting the L-asp dose response data in Fig. 3A to the Michaelis-Menton equation and fitting the Na^+ dose response data in Fig. 3B to the Hill equation. The values are averaged from at least 3 datasets and error indicates s.e.m. Dissociation constants for L-asp binding were derived from fitting the data in Fig. 3C to a single site binding model. The values shown are the average of 2 separate triplicate data sets and the error represents the range.

Figure 1

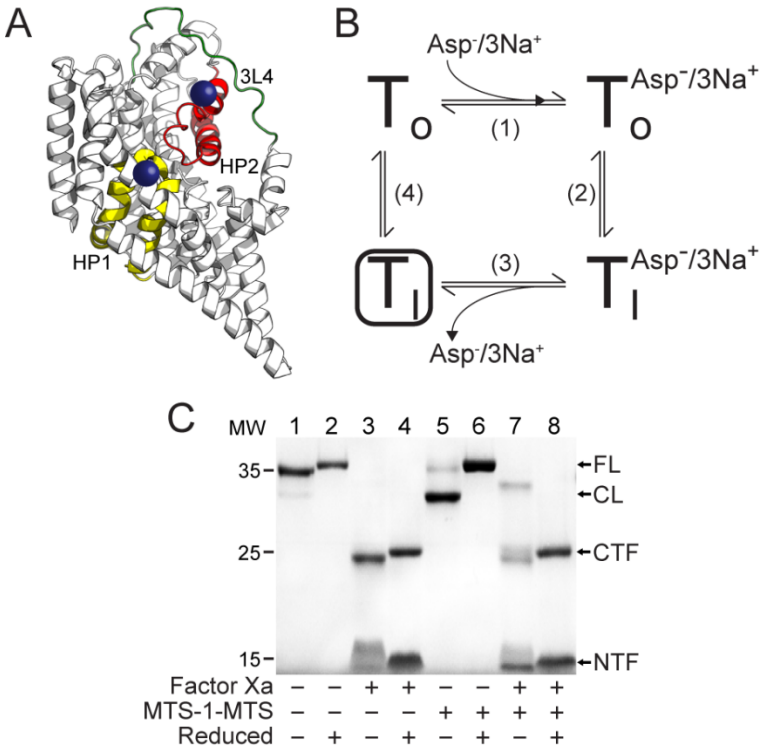
A
3L4
HP2
HP1
B
Asp-/3Na+
To
(1)
To
Asp-/3Na+
(4)
(2)
(3)
Ti
Ti
Asp-/3Na+
Asp-/3Na+
C
MW 1 2 3 4 5 6 7 8
35
25
15
FL
CL
CTF
NTF
Factor Xa – – + + – – + +
MTS-1-MTS – – – – + + + +
Reduced – + – + – + – +

Figure 2

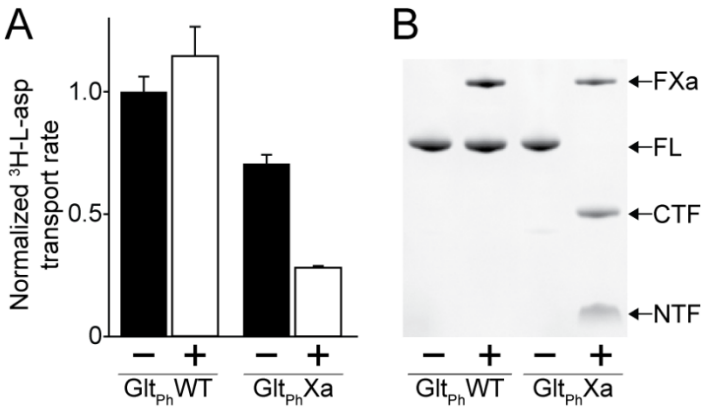
A
B
Normalized ^{3}H-L-asp transport rate
1.0
0.5
0
− + − +
Glt_{Ph}WT
Glt_{Ph}Xa
FXa
FL
CTF
NTF

Figure 3

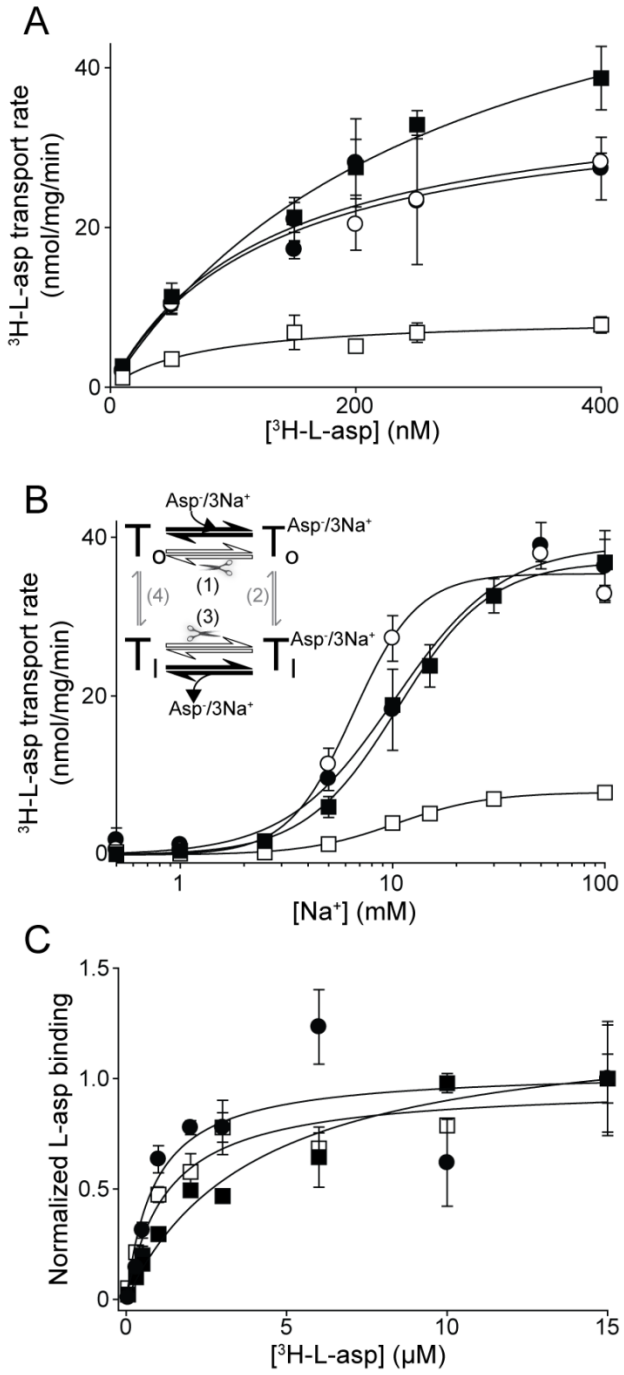
A
^{3}H-L-asp transport rate (nmol/mg/min)
40
20
0
0
200
400
[^{3}H-L-asp] (nM)
B
Asp$^-$/3Na$^+$
T_o
Asp$^-$/3Na$^+$
T_o
(1)
(2)
(3)
(4)
T_i
Asp$^-$/3Na$^+$
T_i
Asp$^-$/3Na$^+$
^{3}H-L-asp transport rate (nmol/mg/min)
40
20
0
1
10
100
[Na$^+$] (mM)
C
Normalized L-asp binding
1.5
1.0
0.5
0
0
5
10
15
[^{3}H-L-asp] (μM)

Figure 4

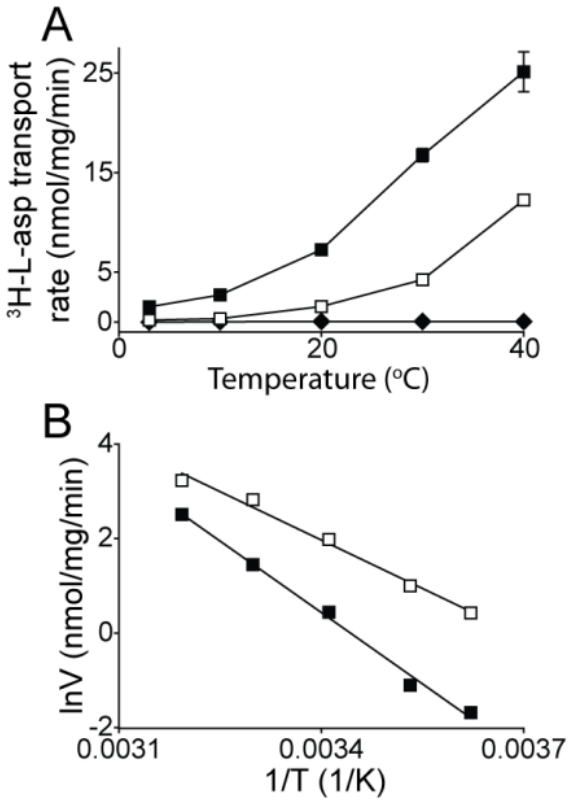
A
^{3}H-L-asp transport rate (nmol/mg/min)
25
15
5
0
0
20
40
Temperature (°C)
B
lnV (nmol/mg/min)
4
2
0
-2
0.0031
0.0034
0.0037
1/T (1/K)

Figure 5

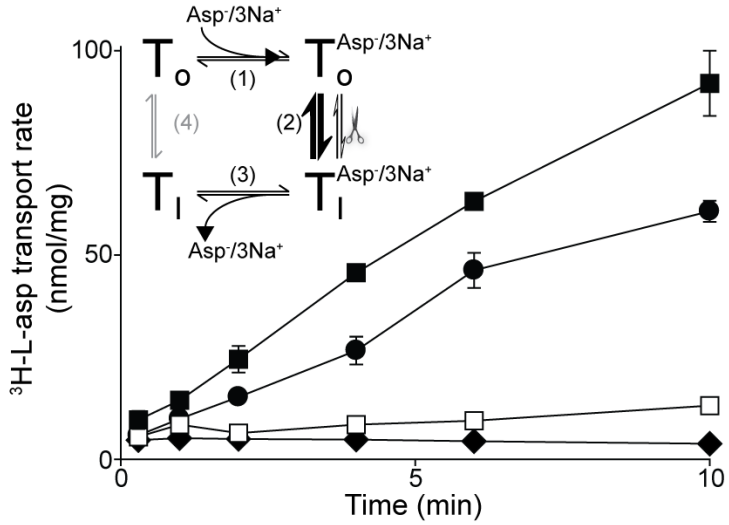
Asp-/3Na+
To
(1)
Asp-/3Na+
To
(4)
(2)
(3)
Asp-/3Na+
TI
TI
Asp-/3Na+
3H-L-asp transport rate (nmol/mg)
100
50
0
0
5
10
Time (min)

Figure 6

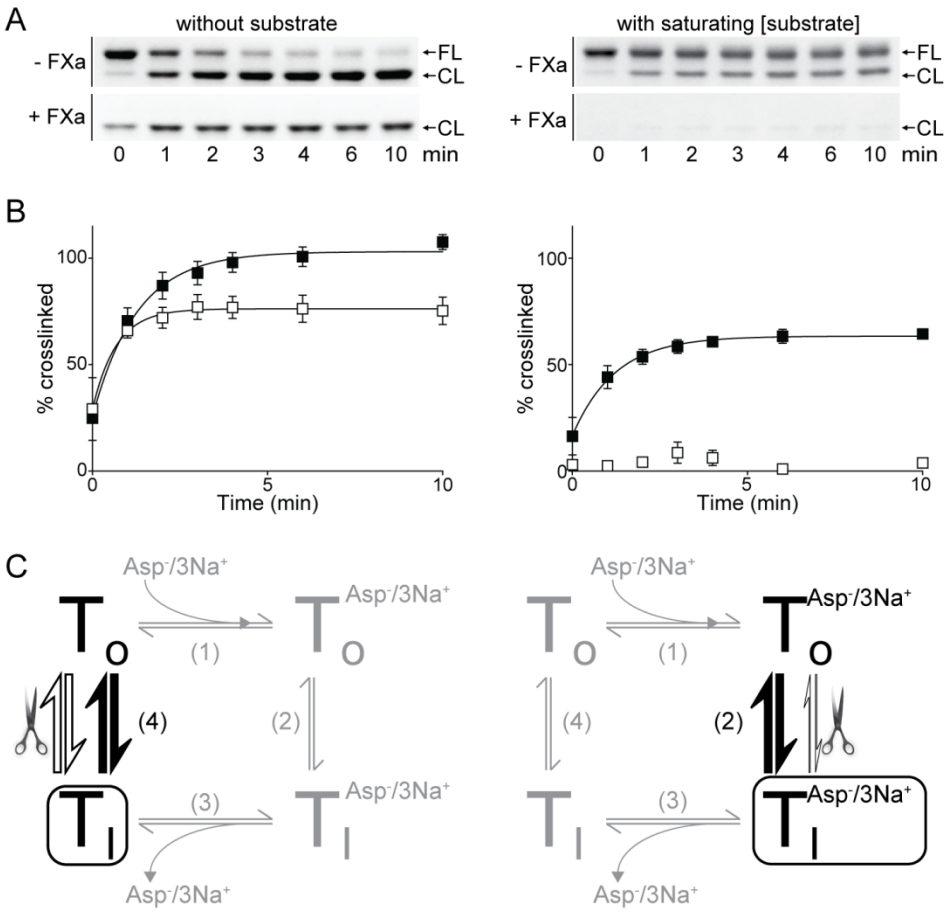
A
without substrate
with saturating [substrate]
- FXa
+ FXa
←FL
←CL
0 1 2 3 4 6 10 min
B
% crosslinked
Time (min)
C
Asp-/3Na+
(1)
(2)
(3)
(4)
To
Ti

Figure 7

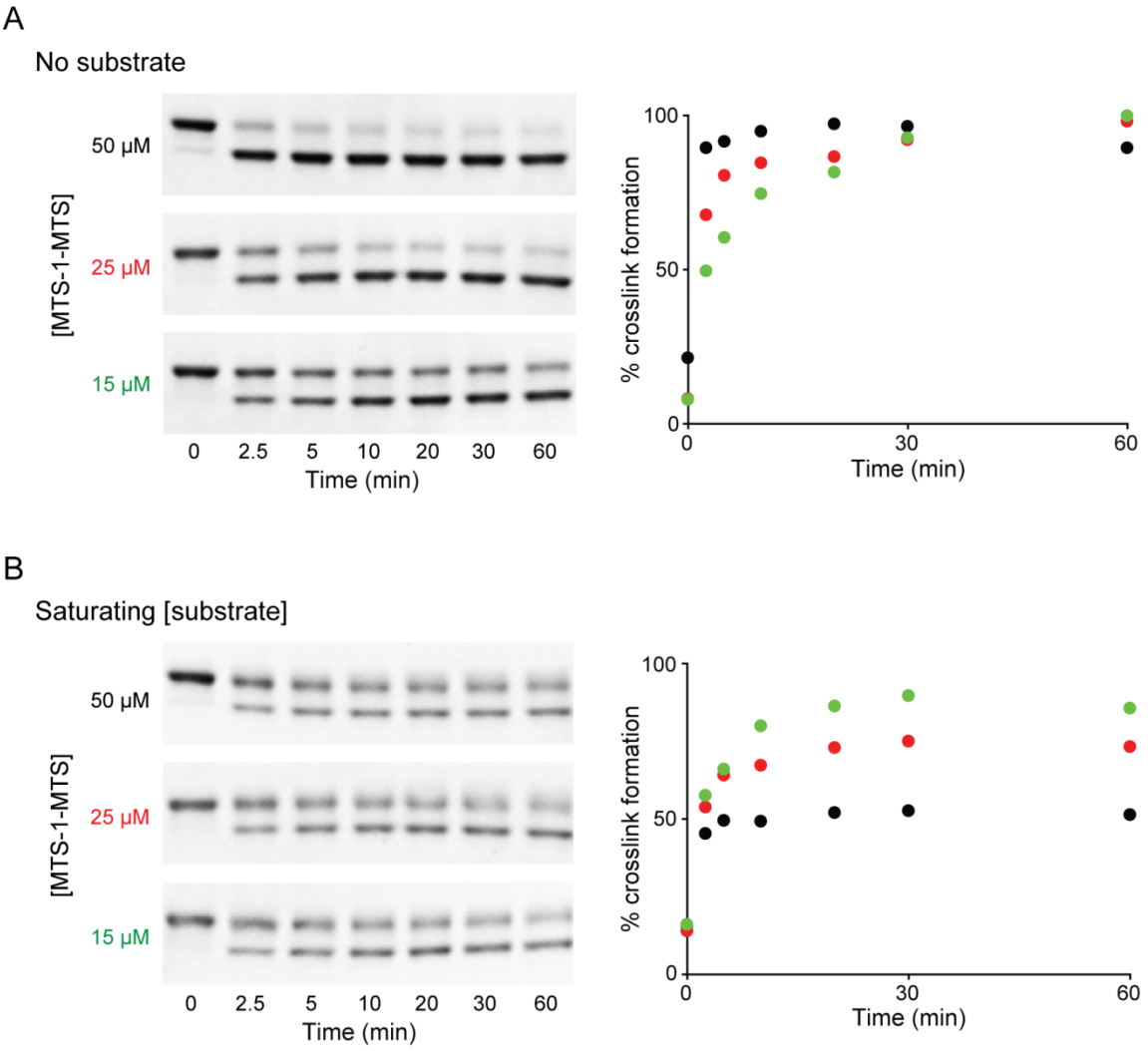
A
No substrate
50 μM
25 μM
15 μM
[MTS-1-MTS]
0 2.5 5 10 20 30 60
Time (min)
% crosslink formation
100
50
0
0 30 60
Time (min)
B
Saturating [substrate]
50 μM
25 μM
15 μM
[MTS-1-MTS]
0 2.5 5 10 20 30 60
Time (min)
% crosslink formation
100
50
0
0 30 60
Time (min)

Figure 8

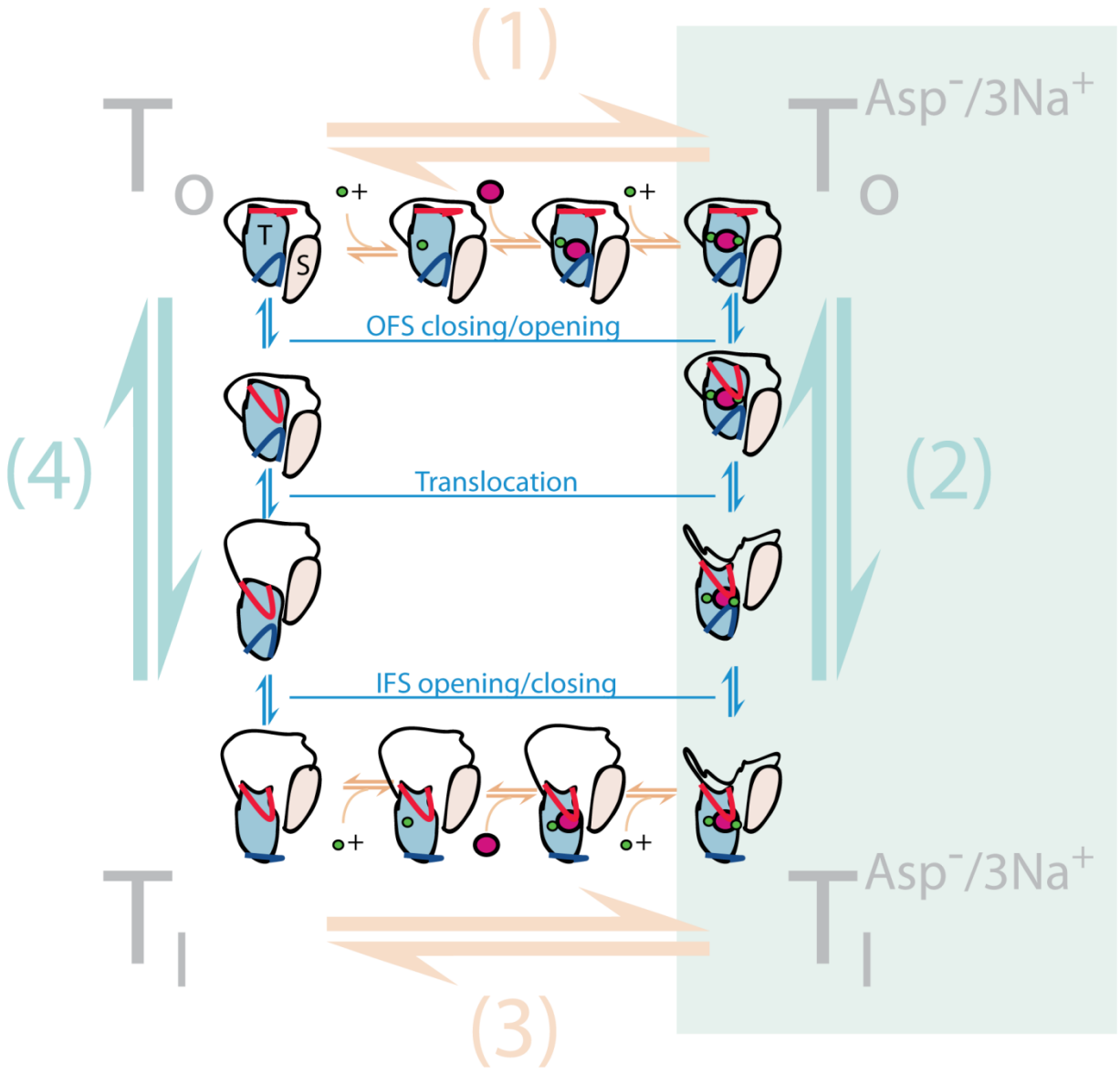
(1)
T_O
$Asp^-/3Na^+$
T
S
OFS closing/opening
(4)
Translocation
(2)
IFS opening/closing
T_I
$Asp^-/3Na^+$
(3)